AIAA SciTech
5-9 January 2015, Kissimmee, Florida
53rd AIAA Aerospace Sciences Meeting

Instability and Transition Experiments in the Boeing/AFOSR Mach 6 Quiet Tunnel

Gregory R. McKiernan*, Brandon C. Chynoweth*, and Steven P. Schneider†
School of Aeronautics and Astronautics
Purdue University
West Lafayette, IN 47907-1282

This paper presents results for two projects in the Boeing/AFOSR Mach 6 Quiet Tunnel (BAM6QT) at Purdue University. The first project uses a 3-meter arc flared cone geometry to measure the second-mode instability. Pressure fluctuation data are compared to TSP images to determine relationship between the magnitude of pressure fluctuations and the heating rate experienced by the model. The RIM roughness is used to alter the magnitude of the pressure fluctuations. Secondly, a pulsed jet perturber was modified to introduce turbulent spots to the BAM6QT nozzle wall boundary layer. Characterization of the valve was completed in order to determine the pulse durations and repeatability. The spot measurements were taken using Kulite pressure sensors.

Nomenclature

f	frequency
M	Mach number
p	pressure
Re	Reynolds number
T	Temperature
x	model axial coordinate
z	Tunnel axial coordinate

Subscripts

0	stagnation condition
i	initial condition
wall	wall condition

Abbreviations

BAM6QT	Boeing/AFOSR Mach-6 Quiet Tunnel
TSP	Temperature-Sensitive Paint
PSD	Power-Spectral Density
RIM	Rod Insertion Method

*Research Assistant. Student Member, AIAA
†Professor. Associate Fellow, AIAA

I. Introduction

A. Hypersonic Laminar-Turbulent Transition

The prediction of laminar to turbulent transition of hypersonic boundary layers has major implications for the design of vehicles, but the underlying mechanisms that cause this transition are poorly understood. Hypersonic laminar-turbulent boundary-layer transition affects heat transfer, separation, skin friction and several other boundary layer properties. The ability to predict or control this transition would lead to more efficient and accurate designs of hypersonic vehicles. Conventional hypersonic tunnels have noise levels between 1-4%. These noise levels will cause transition to occur earlier than in quiet flow and can be more than an order of magnitude greater than in flight. Quiet wind tunnels produce freestream noise levels of less than 0.1% and provide test conditions that can be used to study laminar-turbulent transition at noise levels similar to flight. Transition mechanisms present in low noise environments can be changed or missed in high-noise environments.

B. The Boeing/AFOSR Mach-6 Quiet Tunnel

The Boeing/AFOSR Mach-6 Quiet Tunnel (BAM6QT), shown in Figure 1, is the largest operational hypersonic quiet wind tunnel in the world. The BAM6QT is a Ludweig tube design incorporating a long driver tube with a converging-diverging nozzle at the downstream end. To operate the tunnel the driver tube section is filled to the desired pressure and the tank pumped to vacuum. A pair of diaphragms is then burst causing an expansion fan to propagate upstream. The expansion fan reflects between the end of the driver tube and the contraction section. These reflections produce a quasi-static drop in stagnation pressure throughout the run.

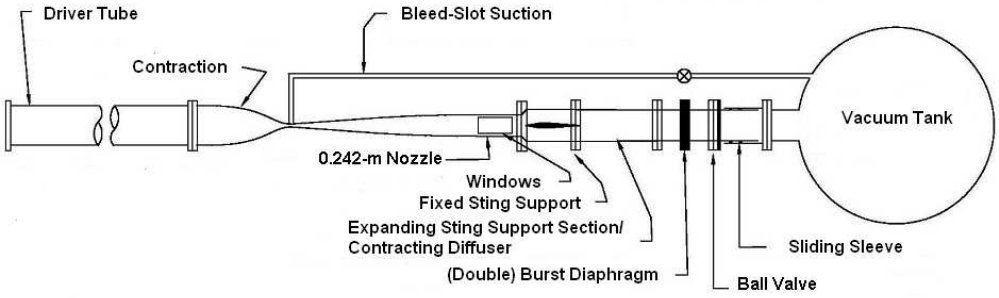

Figure 1. Schematic of Boeing/AFOSR Mach 6 Quiet Tunnel.

The BAM6QT is able to produce noise levels on the order of 0.05% for stagnation pressures up to 170 psia. The BAM6QT uses several features to produce this low noise environment. A suction slot upstream of the throat can be opened to the vacuum tank to remove the boundary layer from the nozzle wall. This allows a fresh laminar boundary layer to begin at the throat. If the suction slot is not used the BAM6QT can operate with noise levels near 3%. This noise level is typical of conventional hypersonic wind tunnels. The divergent portion of the nozzle is polished to a mirror finish in order to avoid any roughness disturbing the boundary layer. In addition the divergent portion is very long in order to reduce the effect of the Görtler instability. Very fine air filters are used to remove any particles in the driver tube large enough to damage the mirror finish.

In the past six months five students have completed theses at the BAM6QT and our group is currently rebuilding a skilled staff. Amanda Chou completed research on receptivity measurements using a laser perturbation system.[1] Chris Ward looked into the crossflow instability and transition at angles of attack.[2] Ryan Henderson completed an investigation of crossflow transition at low angles of attacks.[3] Roger Greenwood

studied entropy layer instabilities on a cone-ogive-cylinder.[4] Dennis Berridge's thesis on the calibration of PCB132A31 pressure sensors in a shock tube is currently being written and will be published in 2015.[5]

II. Transition and Instabilities Measurements on a Flared Cone

A. The Flared Cone Models

The first flared cone fabricated and tested by Chou[6] has a 4-inch base diameter, and is therefore referred to as the 4-inch flared cone. It consists of two pieces, a nosetip and a frustum. The stainless steel nosetip used in the present experiments is 17 cm long with a nose radius of 136 μm (0.005 inches) and an initial opening half-angle of approximately 1.5°. The nosetip radius was measured using a Zygo ZeGage 3-D optical surface profiler. The opening angle was evaluated by taking a picture of the nosetip with a Moticam 3 megapixel camera attached to a microscope. The picture was imported into SolidWorks and the angle was evaluated. The frustum is made of aluminum and is 30.2 cm in length with sides of a constant arc of 3 meters. The total length of the model is 47.2 cm. Sensor ports are located at distances of 23.0, 28.0, 33.0, 35.6, 38.1, 40.6, 43.2, and 45.0 cm from the nosetip.

A flared cone with a larger base diameter but the same 3-meter circular arc was developed to increase the maximum Reynolds number based on the length of the model. The model consists of a nosetip, a roughness insert, and a frustum as shown in Figure 2. This model will be referred to as the Roughness Insert Cone. The nosetip is 25.4 cm long with a nose radius of 152 μm (0.006 inches) and an opening half-angle of approximately 1.5°. The cone was designed with a space 0.635 cm (0.25 inches) wide between the nosetip and the frustum. This gap is filled with a removable roughness insert that can either be left unmodified to test smooth wall cases, or roughness elements can be added to the surface creating a RIM roughness previously reported on by Chynoweth.[7] The insert allows for testing of both destructive and non-destructive methods of producing roughnesses. The frustum is 25.6 cm long for a total model length of 51.6 cm. Sensors are placed at a distance of 33.9, 36.5, 39.0, 41.6, 44.1, 46.6, and 49.2 cm from the nosetip.

The mean flow around the model was computed using the Stability and Transition Analysis for Hypersonic Boundary Layers (STABL) code developed at the University of Minnesota. A grid was generated for both the 4-inch base cone and the Roughness Insert Cone. The ratio of the surface static pressure to the freestream stagnation pressure was computed for stagnation pressures of 90, 120, 140, and 160 psia. Across this 70 psia range, the ratio at any given stagnation pressure was less than 1% different than the mean value. Therefore, the average of ratio from the four computations was used to calculate pressure ratio on the surface at each discrete sensor location and used in normalization when computing the power spectral densities as described in the following section.

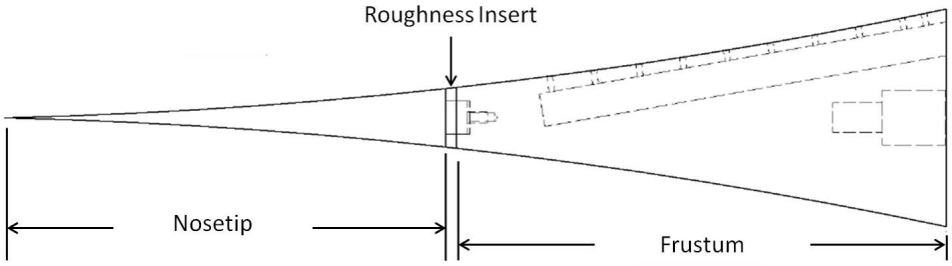

Figure 2. Schematic of the roughness insert cone with a 11.4 cm base diameter.

B. Data Reduction Techniques - Power Spectral Densities and Magnitude Calculations

Pressure fluctuation data were obtained using PCB132A31 pressure sensors. Oscilloscopes produced by the Tektronix Corporation were used to sample the data using Hi-Res mode to improve vertical resolution. Data were collected at sampling rates of either 2 or 5 MHz to satisfy the Nyquist criteria for resolving pressure fluctuations up to 1 MHz. Power spectral densities (PSDs) were computed by employing Welch's method in a MATLAB script. Each PSD was computed over 0.1 second intervals. Special attention was given to ensure that no turbulent bursts were present during the processed intervals. The mean of the voltage is subtracted to eliminate any offset, and then the data are converted to a pressure using the factory calibration of the PCB132A31 sensor. The pressure fluctuation (P') is then normalized by the mean static pressure (P_{mean}) at the sensor location using results obtained from 2-D STABL computations. Power spectra are determined by averaging Fast-Fourier Transformations (FFT) computed using a sliding Blackman window with 50% overlap. The window size used to compute the FFT varied based on the sampling rate for the sensor to maintain a frequency resolution of 2 kHz.

The magnitude of the pressure fluctuation due to the second-mode disturbance was computed by integrating a single PSD. A MATLAB script was written that determines the frequency of the peak PSD value in the range of the expected second-mode frequencies (200 kHz to 400 kHz). The PSD was then numerically integrated over a bandwidth of 200 kHz centered on the peak primary second-mode frequency. These calculations are similar to those performed by Marineau et al.[8] at AEDC Tunnel 9 except a bandwidth of 60 kHz was used in their calculations. The square root of the integrated value is the ratio of pressure fluctuation to the mean pressure, P'/P_{mean}. A sample PSD is shown in Figure 3. The portion in red is integrated over to determine the magnitude of the pressure fluctuation. Using these techniques to compute the power spectra and the magnitude of the pressure fluctuations, it was possible to extract up to seven slices of data 0.1 seconds in length over the duration of a single run for a given sensor.

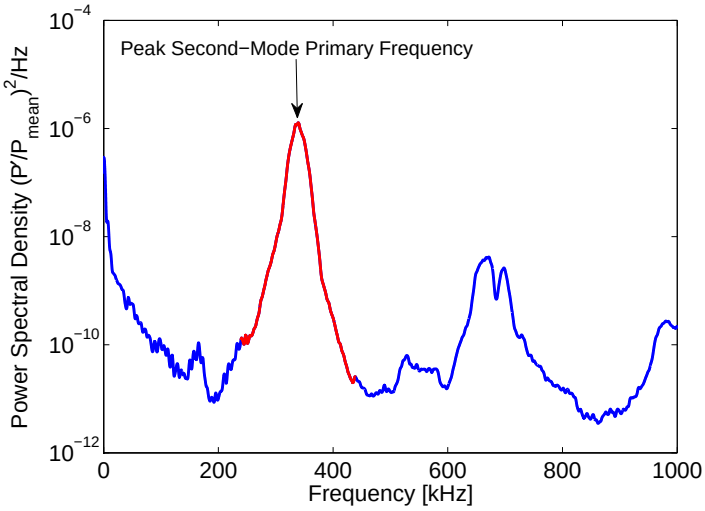

Figure 3. PSD of PCB132 sensor located 39.0 cm from the nosetip of the Roughness Insert Cone at a unit Re = 12.4×10^6/m. Portion in red is the bandwidth used for magnitude calculation.

C. Heating Phenomena and the Connection to Pressure Fluctuations

Experiments on the 4-inch flared cone shed light on the heating experienced by the surface of the cone and its relationship to the magnitude of the pressure fluctuations. A typical temperature sensitive paint (TSP) image is shown in Figure 4. The hot-cold-hot streaks were observed and commented on in Reference 7, but pressure fluctuation data were not presented. Computations by Fasel and Sivasubramanian show that the heating pattern can be attributed to the growth, saturation, and breakdown of the second-mode instability in the boundary layer.[9]

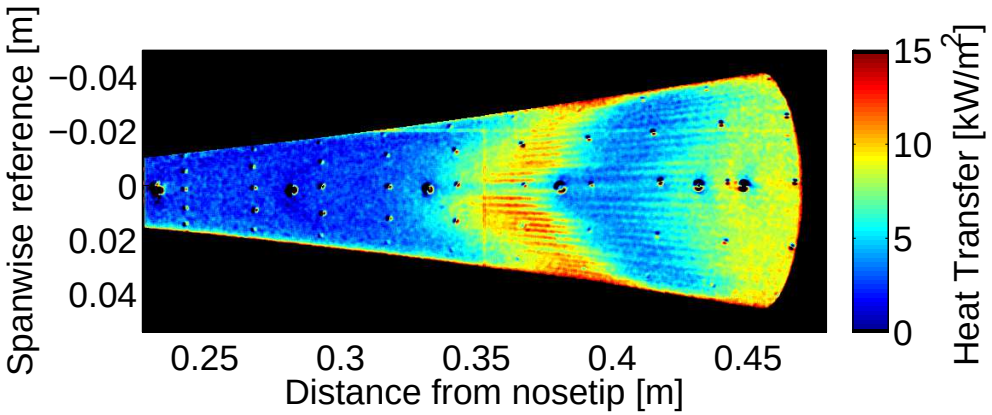

Figure 4. Typical TSP image of the 4-inch base cone at a unit Re = 10.8×10^6/m, $P_0 \approx 140$ psia . Flow is from left to right.

Eight runs were performed under quiet condition in the BAM6QT. The initial stagnation pressure ($P_{0,i}$) was increased from 100 to 170 psia in 10 psia increments. It was observed that the sensor located at x = 40.6 cm encountered nearly all portions of the hot-cold-hot streak heating pattern. The magnitude of the pressure fluctuations measured by this sensor versus the Reynolds number based on the distance from the nosetip to the sensor (Re_x) is shown in Figure 5(a). For each run there are seven data points corresponding to seven time slices during the run. As the stagnation pressure drops in the BAM6QT facility during a run, the Re_x also decreases. Figure 5(b) shows the PSD for five runs in the same entry. The data are taken 1 second into the run, and each PSD corresponds to a data point in Figure 5(a) outlined with a black diamond.

During Run 711 the maximum amplitude of the peak second-mode instability and the largest pressure fluctuations were recorded. Increasing the stagnation pressure further causes the amplitude of the peak second-mode PSD to decrease. A spreading of the bandwidth of the primary second-mode frequency is also observed. For all runs presented, second and third harmonics can be seen at approximately 600 kHz and 900 kHz.

Figure 6(a) through 6(d) are TSP images of Runs 709, 711, 713, and 714 corresponding temporally during each run to the data in Figure 5(a) outlined with black diamonds. All pressure fluctuation data in Figure 5(a) were collected from the sensor located at x = 40.6 cm and approximately 0 meter in the spanwise reference in the TSP images.

The magnitude of the pressure fluctuation begins to increase upstream of the first set of streaks. The streaks move upstream as the Reynolds number increases exposing the sensor to a variety of flow conditions. When the sensor is fully engulfed in the upstream set of streaks, the pressure fluctuations reach their maximum magnitudes with values near 25% of the mean pressure. The magnitude of the pressure fluctuations begins to decay as the region of lower heating between the portions of increased heat transfer passes over the sensor.

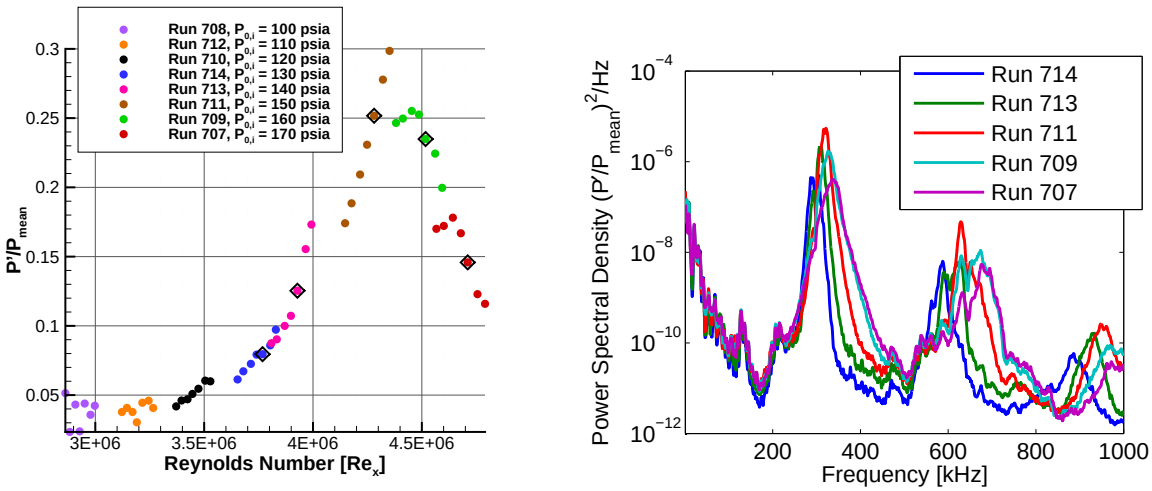

(a) (b)

Figure 5. (a) Magnitudes of pressure fluctuations due to the second-mode instability at a sensor location 40.6 cm from the nosetip. (b) Power spectra of points outlined with black diamonds in (a).

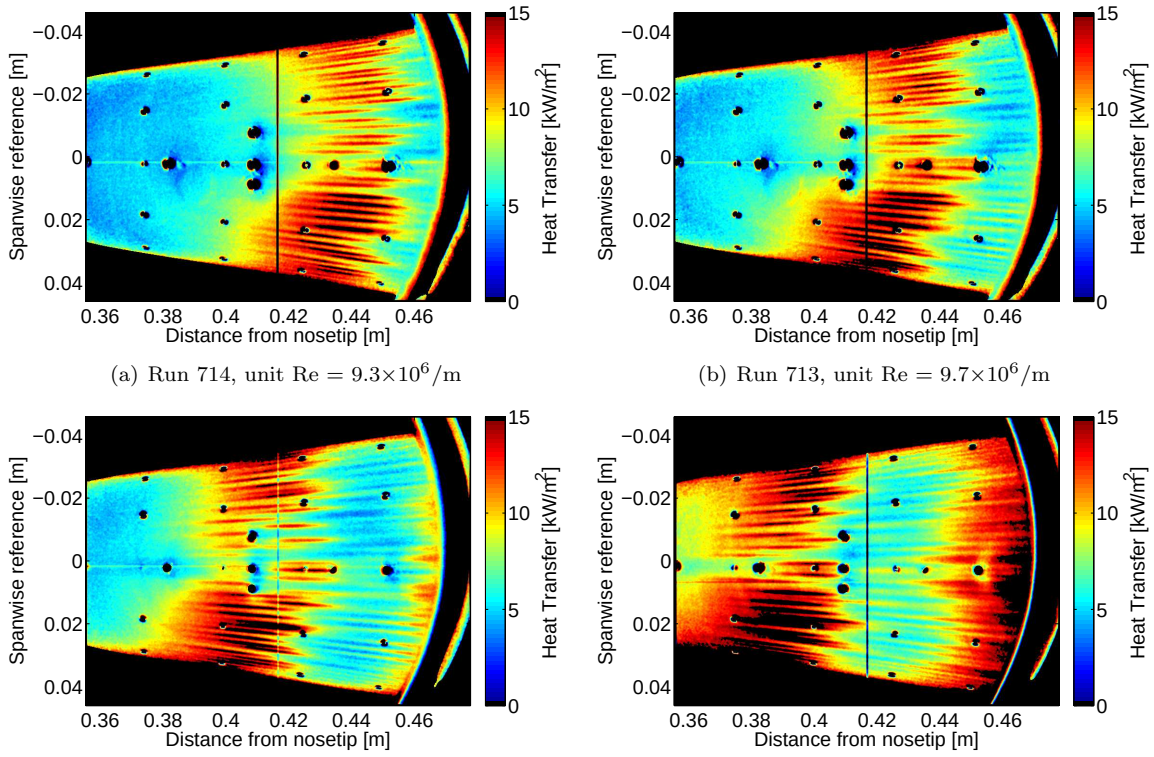

(a) Run 714, unit Re = 9.3×10^6/m

(b) Run 713, unit Re = 9.7×10^6/m

(c) Run 711, unit Re = 10.5×10^6/m

(d) Run 709, unit Re = 11.1×10^6/m

Figure 6. TSP images at four different stagnation pressures. Data presented in Figure 5(a) are from the sensor at a distance from the nosetip of 40.6 cm and a spanwise reference of approximately 0.

D. Pressure Fluctuation Experiments on the Roughness Insert Cone

The Roughness Insert Cone was first tested without TSP. Figure 7 shows the magnitude of the pressure fluctuations as measured by 7 sensors on the surface of the cone for three different runs. Note that the abscissa is the Reynolds number based on the distance of the sensor from the nosetip. Seven data points were extracted from the data for each sensor, resulting in 49 data points for a single run. The solid symbols in Figure 7 show that the maximum pressure fluctuation is approximately 25% of the mean pressure on the surface of the cone for three different initial stagnation pressures without TSP.

TSP was applied and measurements were made at the same condition. Figure 7 compares the results without paint (solid symbols) to results with TSP (empty symbols). The magnitude of the peak pressure fluctuations is attenuated at the lowest initial stagnation pressure of 110 psia. At an initial stagnation pressure of 150 psia, the maximum magnitude difference is less than 15%.

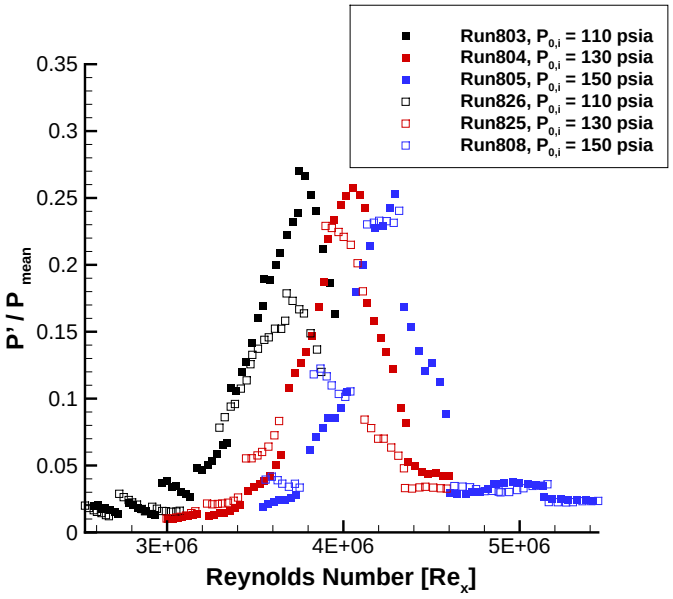

Figure 7. Comparison of pressure fluctuation magnitudes with TSP (empty symbols) versus without TSP (solid symbols) at three different $P_{0,i}$.

Two experiments were performed with the RIM roughness varying the height of the top of the rod above the surface. Thirty brass rods with a diameter of 838 μm were evenly spaced 12° apart around the circumference of each insert. The two roughness heights were 254μm (0.010 inches) and 381 μm (0.015 inches). Figure 8(a) compares the pressure fluctuations measured with and without RIM roughnesses for an initial stagnation pressure of 130 psia. Figures 8(b), 8(c), and 8(d) show the TSP images corresponding to the pressure fluctuation data. The 254 μm roughness produces a peak fluctuation about 5% larger in magnitude than the cone tested without roughness. The peak magnitude is measured by the same sensor located 44.1 cm from the nosetip. Comparing Figure 8(b) to Figure 8(c), it can be seen that a streak of increased heating is passing over this sensor for both cases. Testing with the 381 μm high roughness, the peak pressure fluctuation has been attenuated by nearly 60%, but it is unclear whether the actual maximum value has been measured. In addition, investigation of the TSP image shows that the sensor at x = 44.1 cm does not have a streak passing directly over it.

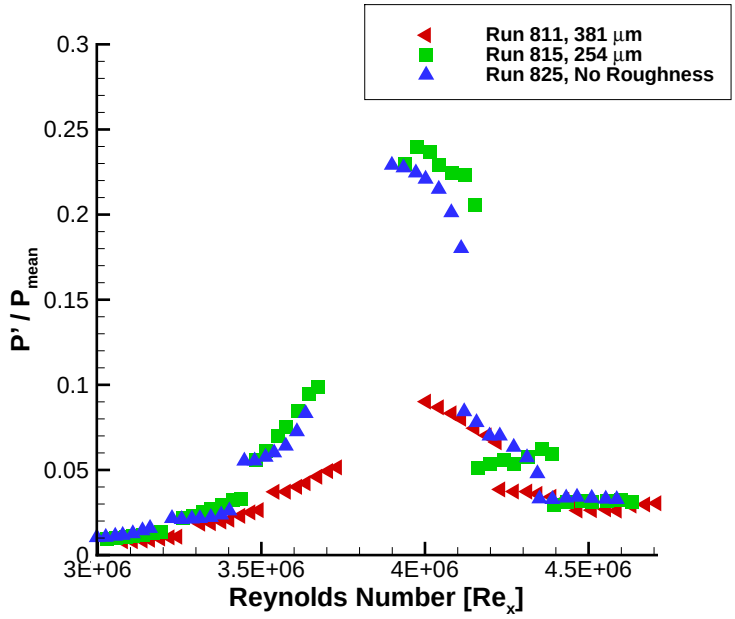

(a)

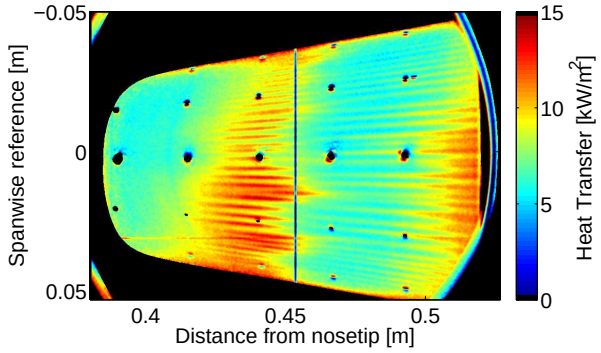

(b) Run 825, No Roughness.

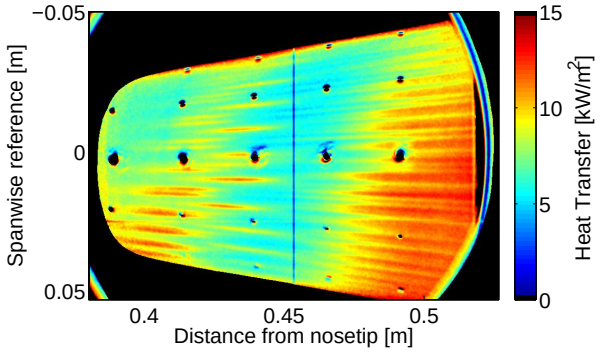

(c) Run 815, Roughness Height = 254 μm

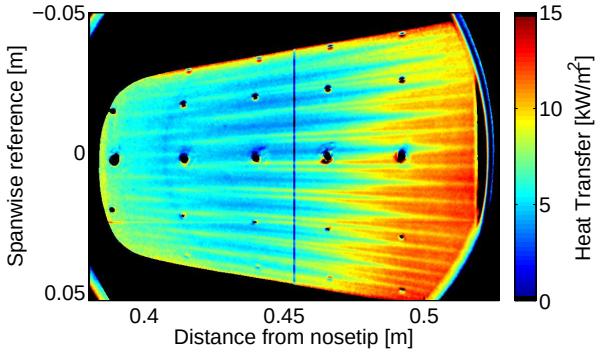

(d) Run 811, Roughness Height = 381 μm.

Figure 8. Comparison of pressure fluctuations on the Roughness Insert Cone with and without the RIM roughness along with corresponding TSP images at an initial stagnation pressure of 130 psia.

In Figure 9(a) it can be seen that the first region of increased heating is composed of a pair of streaks formed directly downstream from each roughness element. In between the streak pairs, a single streak beings to form at approximately x = 43 cm. Rotating the roughness insert by 6°, it was possible to expose the sensor ray to a different heating pattern. Figure 9(a) is a TSP image with the original test configuration. In figure 9(b), the RIM roughness is rolled by 6° . Both runs start at an initial stagnation pressure of 130 psia. It can be seen that the sensor at x = 44.1 cm is now directly downstream from a streak pair, but no longer subjected to increased heating rates. The pressure fluctuation magnitudes are compared in Figure 9(c). It is clear that the peak pressure fluctuation was not measured during the test with the insert rolled 6°, but general trends indicate that a peak should occur between a Re_x of 3.7×10^6 and 4×10^6. Future testing will focus on the collection of data to more fully characterize the pressure fluctuations. Additional sensors will be added to increase the likelihood that the peak pressure fluctuation will be captured.

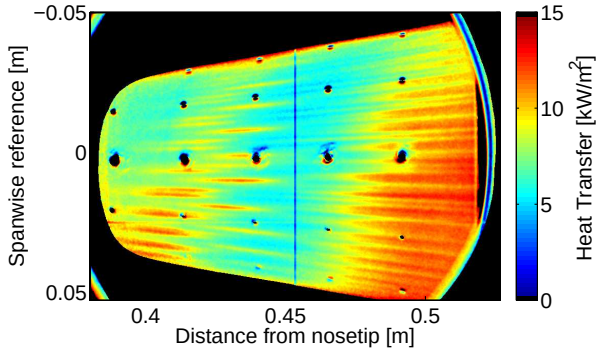

(a) Run 815, Roughness Height = 254 μm.

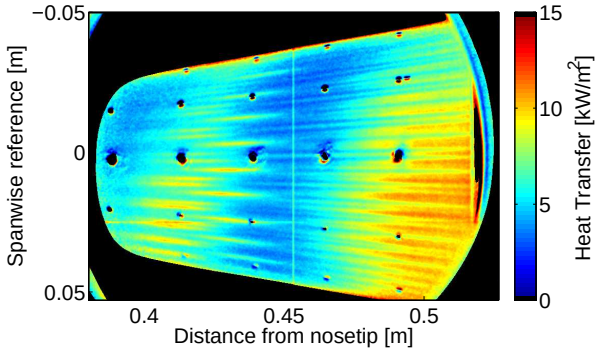

(b) Run 824, Roughness Height = 254 μm, RIM roughness rolled 6°.

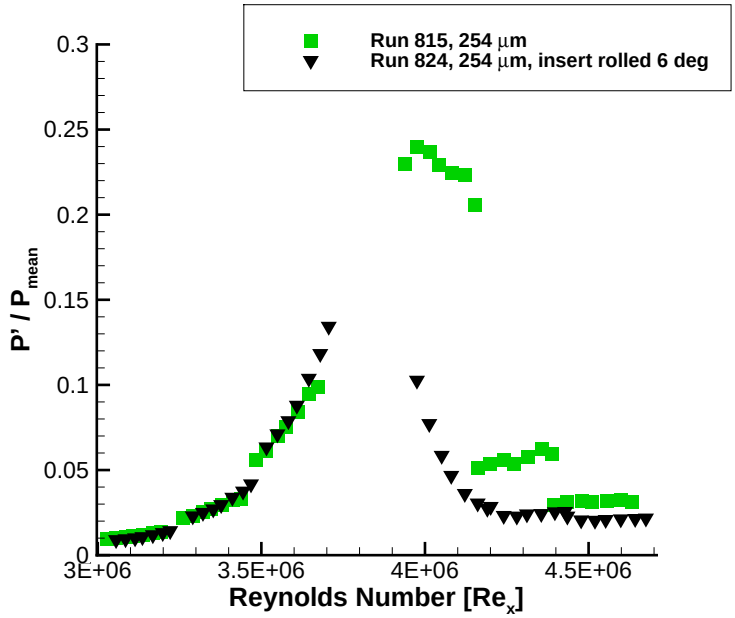

(c)

Figure 9. (a),(b) TSP images showing streaks of increased heating relative to sensor position. (c) Pressure fluctuation magnitudes measured during Runs 815 and 824.

III. A Pulsed Jet to Produce Turbulent Spots at Mach 6

A. Brief Background and Previous Experiments

Hypersonic vehicles are subject to high amplitude pressure fluctuations during boundary layer transition due to the intermittent passage of turbulent spots. In order to accurately predict the transitional pressure field along a body, an intermittency model of transition could be used.[10] Turbulent spots appear randomly at the transition onset location and grow as they convect downstream. The length of the transitional region can be determined if the growth and formation rates of the spots are known. Casper measured several turbulent spot characteristics using a pulsed glow perturber in the BAM6QT.[11,12] Casper was able to measure the low frequency footprint and the leading and trailing edge convection rates of a turbulent spot. However a perturber of a higher amplitude is needed to develop fully mature turbulent spots in the BAM6QT. For this reason Abney designed a pulsed jet perturber to introduce a transverse jet into the nozzle wall boundary layer of the BAM6QT.[13]

B. Current Results

The pulsed jet perturber is based on a Parker Hannafin Corporation 009-1669-900 pulse valve. The valve was originally designed for spectroscopy experiments for use within a vacuum chamber. This off the shelf component is well suited to both the low static pressure and the high pre-run pressure during operation of the BAM6QT. A schematic of the internal components of the valve is shown in figure 10(a). Abney attempted to shorten the duration of the pulse by machining a flat onto the poppet. This countersink is supposed to reduce the mass flow of the air released from the valve, subsequently reducing duration.[13] These modifications are shown in figure 10(b). Due to the high speeds within the BAM6QT the ideal pulse time would 10-100 μs.

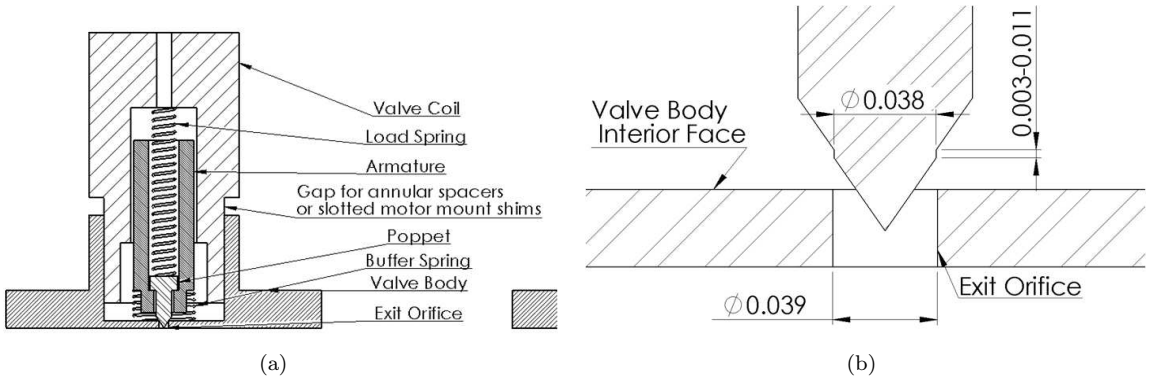

Figure 10. (a) Internal components of the Parker Hannafin 009-1699-900 valve. (b) Dimensions of the poppet modifications.

Previous experiments have shown the alignment of the valve is very difficult to maintain during testing. The coarse threading that controlled the armature deflection limited the operating range to a 30° rotation. Figure 11 shows the custom housing for the valve designed by Robin Snodgrass of the AAE machine shop. This housing is intended to help maintain a consistent and precise alignment by means of a micrometer controlling the deflection of the armature.

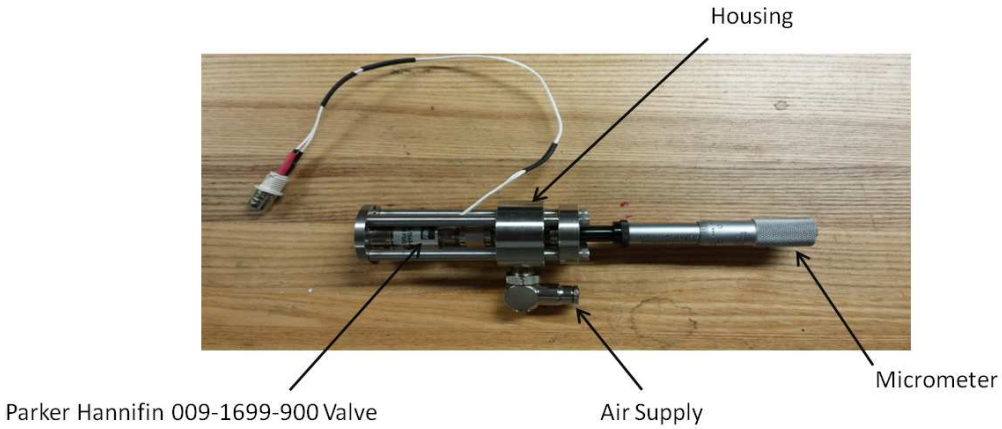

Figure 11. Modified Parker Hannafin Valve with alignment housing.

Repeatability of the valve was tested in a vacuum test cell created from the old BAM6QT diffuser section and in the BAM6QT itself. All tunnel runs were completed at Re $\approx$ 8.0×10^6/m. The test cell was evacuated to match the low static pressures present during tunnel runs and a Kulite was installed directly in line with the impinging jet. Figure 12(a) shows the pulse durations for four consecutive valve openings within the test cell. The standard deviation for all micrometer deflections were below 1% of the pulse duration. Figure 12(b) shows the repeatability of the valve after being disassembled and reassembled within the test cell and the BAM6QT. The tunnel measurements were taken at the furthest upstream sensor which is 0.13 m downstream of the valve. The distance between the valve and the sensor allows the spot to grow as it convects downstream. Thus, the tunnel pulse durations are expected to be slightly longer than test cell durations. As the micrometer pushes the armature further into the coil the pulses become less repeatable. At a 0.936 in micrometer deflection the pulse durations vary by several hundred microseconds. If the pulses present for a 0.935 micrometer deflection are fully turbulent, the pulse length of the turbulent spot could be known within 100 μs .

Testing was completed to determine if the shorter and more repeatable micrometer setting produced fully developed turbulent spots. Figure 13(a) shows the pressure traces of the valve offset at values proportional to the axial distance from the throat of the nozzle (z). The corresponding PSD of the pulse is found in figure 13(b). The less repeatable valve configuration (0.936" micrometer deflection) is shown in Figures 14(a) and 14(b). Both spectra show broadband noise indicative of turbulent flow. The pressure traces show the 0.935" deflection creates a larger burst than the 0.936" micrometer deflection. It seems the micrometer deflections that produce the largest disturbances are the most repeatable.

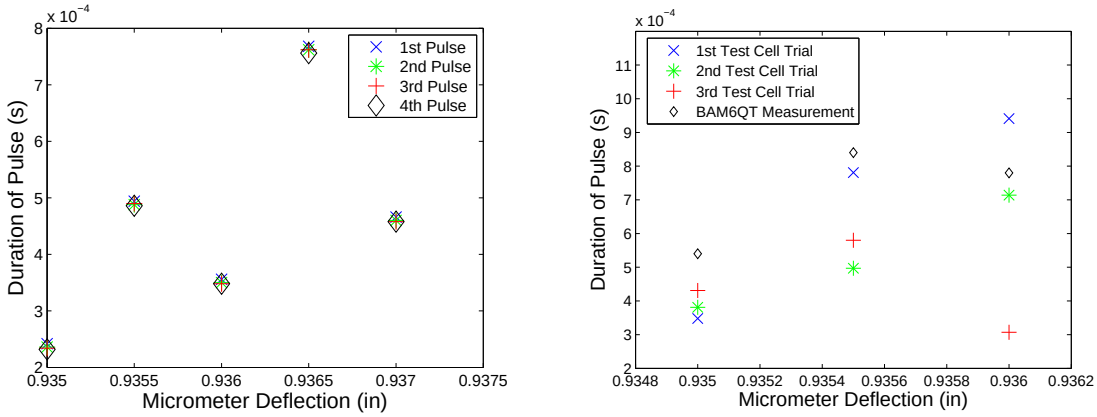

(a) (b)

Figure 12. (a) Pulse durations of consecutive pulses for several micrometer deflections. (b) Average pulse durations after disassembly and reassembly of the valve for repeated conditions.

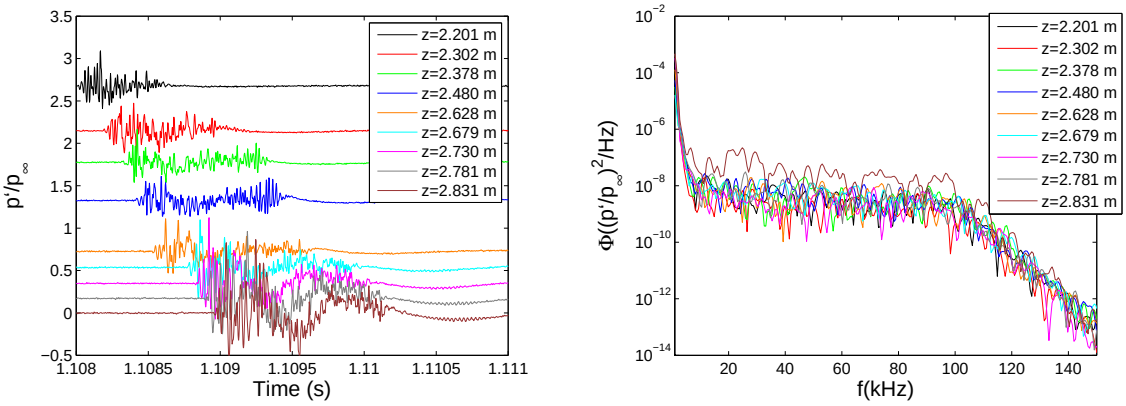

(a) (b)

Figure 13. (a) Normalized pressure trace at Re $\approx$ 8.0 $\times 10^6$/m with the stock poppet and 0.935" micrometer deflection. (b) Power spectral density of the normalized pressure traces.

An attempt to find the shortest pulse duration was completed for all the modified poppet designs. Figure 15 shows the shortest pulse durations found for the five different poppet countersinks. A 0.009 in countersink produced the shortest pulses at approximately 300μs. This duration will produce a turbulent spot approximately 12 inches in length at Mach 6. When tested in the BAM6QT the same trend was observed with the shortest pulses being below 500μs and produced by the 0.009" countersink.

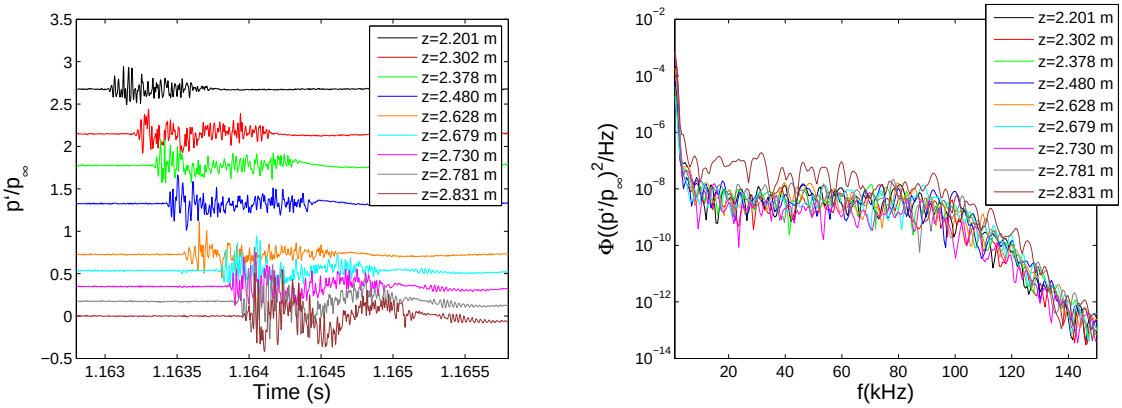

(a) (b)

Figure 14. (a) Normalized pressure trace at Re ≈ 8.0 $\times 10^6$/m with the stock poppet and 0.936" micrometer deflection. (b) Power spectral density of the normalized pressure traces.

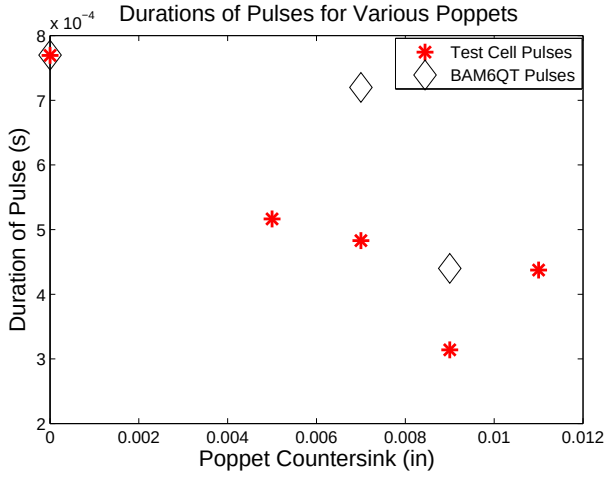

Figure 15. Duration of pulses with varying poppet countersinks.

IV. Conclusion

1. Peak Second-mode pressure-fluctuation magnitudes were measured to be 25% at breakdown on the flared cone geometry. The peak fluctuations occur at the downstream end of the first region of increased heating. Using the RIM roughness technique, the peak magnitude is attenuated by 60% with a roughness height of 381 μm. A roughness height of 254 μm resulted in nearly the same peak pressure fluctuation magnitude as the model without any roughness. Future tests will focus on testing different RIM roughness spacings and element heights to determine the magnitude of the pressure fluctuations at breakdown under different conditions.

2. A new design of a pulsed valve was developed and shown to be an improvement on previous attempts to produce turbulent spots in the BAM6QT. Pulse durations of 300μs have been created in controlled testing outside the tunnel. Tests within the tunnel produced pulses below 500μs. The reliability of the valve is dependent on the deflection of the armature within the solenoid. Further analysis needs to be completed to determine the repeatability of the shortest pulses with the 0.009" poppet countersink.

However, it seems unlikely that this technique can produce the desired 100μs pulses.

V. Acknowledgements

This research is funded by the Air Force Office of Scientific Research under grant number FA9550-12-1-0167. Brandon Chynoweth is funded under a NDSEG Fellowship. Heath Johnson and Graham Candler at the University of Minnesota were very helpful in installing STABL on our Purdue computer and assisting us in running the code.

References

[1]Chou, A., *Mach-6 Receptivity Measurements of Laser-Generated Perturbations on a Flared Cone*, Ph.D. thesis, Purdue University, West Lafayette, Indiana, August 2014.

[2]Ward, C. A. C., *Crossflow Instability and Transition on a Circular Cone at Angle of Attack in a Mach-6 Quiet Tunnel*, Ph.D. thesis, Purdue University, West Lafayette, Indiana, October 2014.

[3]Henderson, R. O., *Crossflow Transition at Mach 6 on a Cone at Low Angles of Attack*, Master's thesis, Purdue University, West Lafayette, Indiana, October 2014.

[4]Greenwood, R. T., *Measurements of Entropy-Layer Instabilities over Cone-Ogive-Cylinders at Mach 6*, Ph.D. thesis, Purdue University, West Lafayette, Indiana, December 2014.

[5]Berridge, D., *To Appear*, Ph.D. thesis, Purdue University, West Lafayette, Indiana, 2015.

[6]Chou, A., *Characterization of Laser-Generated Perturbations and Instability Measurements on a Flared Cone*, Master's thesis, Department of Aeronautics and Astronautics, Purdue University, West Lafayette, IN, 2010.

[7]Chynoweth, B., Ward, C., Greenwood, R., McKiernan, G., Fisher, R., and Schneider, S., "Measuring Transition and Instabilities in a Mach 6 Hypersonic Quiet Wind Tunnel," AIAA Paper 2014-2643, June 2014.

[8]Marineau, E. C., Moraru, C. G., Lewis, D. R., Norris, J. D., Lafferty, J. F., and Johnson, H. B., "Investigation of Mach 10 Boundary Layer Stability of Sharp Cones at Angle-of-Attack, Part 1: Experiments," AIAA Paper 2015-1737, January 2015.

[9]Sivasubramanian, J. and Fasel, H. F., "Numerical Investigation of Laminar-turbulent Transition for a Flared Cone at Mach 6," AIAA Paper 2015-0839, January 2015.

[10]Park, S. and Lauchle, G. C., "Wall pressure fluctuation spectra due to boundary-layer transition," *Journal of Sound and Vibration*, Vol. 319, 2009, pp. 1067–1082.

[11]Casper, K. M., Beresh, S., and Schneider, S., "Spanwise Growth of the Turbulent Spot Pressure-Fluctuation Field in a Hypersonic Boundary Layer," AIAA Paper 2011-3873, June 2011.

[12]Casper, K. M., *Pressure Fluctuations Beneath Instability Wave Packets and Turbulent Spots in a Hypersonic Boundary Layer*, Ph.D. thesis, Purdue University School of Aeronautics and Astronautics, August 2012.

[13]Abney, A. D., *A Pulsed Jet for Generation of Turbulent Spots in a Mach 6 Boundary Layer*, Master's thesis, Department of Aeronautics and Astronautics, Purdue University, West Lafayette, IN, 2013.